

Serial MultiView: an efficient approach to mitigating atmospheric spatial-structure errors for VLBI astrometry

JINGDONG ZHANG ^{1,2} BO ZHANG ¹ SHUANGJING XU ^{3,1} MARIA J. RIOJA ^{4,5} RICHARD DODSON ⁴
XIAOFENG MAI ^{1,2,6} AND OLEG TITOV ⁷

¹*Shanghai Astronomical Observatory, Chinese Academy of Sciences, 80 Nandan Road, Shanghai 200030, People's Republic of China*

²*University of Chinese Academy of Sciences, No.19 (A) Yuquan Rd, Shijingshan, Beijing 100049, People's Republic of China*

³*Korea Astronomy and Space Science Institute, 776 Daedeok-daero, Yuseong-gu, Daejeon 34055, Republic of Korea*

⁴*International Centre for Radio Astronomy Research, The University of Western Australia, 35 Stirling Hwy, Crawley, WA, Australia*

⁵*Observatorio Astronómico Nacional (IGN), Alfonso XII, 3 y 5, 28014, Madrid, Spain*

⁶*University of Helsinki, P.O. Box 64, FI-00014, Finland*

⁷*Geoscience Australia, Canberra, ACT, 2601, Australia*

Submitted to AJ

ABSTRACT

Atmospheric propagation errors are a main constraint on the accuracy of Very Long Baseline Interferometry (VLBI) astrometry. For relative astrometry, differential techniques can mitigate these errors, but their effectiveness diminishes with decreasing elevation and increasing angular separations between target and calibrator, among others. The MultiView technique addresses atmospheric spatial-structure errors by observing multiple calibrators around the target and interpolating at the target position, thereby reducing residual atmospheric errors more effectively than phase-referencing with only one calibrator. Conventional MultiView approach involves cyclically observing all calibrators and the target, fitting a phase plane from the phases of all calibrators in each cycle. This approach reduces on-target time and is restricted by the interferometer coherence time. We propose a new approach, serial MultiView, which rotates the phase plane iteratively based on the time series of calibrator residual phases. The new approach eliminates the need to observe all calibrators in each cycle, thus shortening the observing cycle and increasing the proportion of on-target time. Additionally, by incorporating time-domain information in the iterations, phase ambiguities can be accurately and automatically identified. This approach enables efficient high-accuracy differential astrometry and artifact-reduced imaging for astrophysical studies, and we provide a user-friendly tool for it.

Keywords: Radio astrometry — Very long baseline interferometry

1. INTRODUCTION

Very Long Baseline Interferometry (VLBI) provides the highest differential astrometric accuracy at present. The key to this high accuracy is the calibration of the interferometric phase observable. Phase-referencing (PR, [Lestrade et al. \(1990\)](#); [Beasley & Conway \(1995\)](#)) techniques, in short observing the target and a nearby calibrator alternatively or simultaneously, are used for the

calibration. Most of the error terms are canceled out benefiting from the small angular separation between target and calibrator. However, the thermal noise limit of VLBI astrometry has only been reached with PR in a limited number of cases. This is partly because of the residual delay caused by the atmosphere, especially when a close enough calibrator is not available. The atmospheric residual delay includes tropospheric and ionospheric terms, which have a time-varying nature and irregular spatial structures. At higher frequencies, tropospheric turbulence is the dominant term; while at lower frequencies, irregularities in ionospheric plasma density dominate.

The MultiView technique (Rioja et al. 2017) compensates for atmospheric spatial-structure errors through observations of multiple calibrators around the target, and demonstrates a significant astrometric improvement at 1.6 GHz with the potential of wide applicability to many sources. Basically, in MultiView the atmospheric spatial structure is approximated to be a plane (in the simplest case), and the phase correction for the target is interpolated from the phases of three or more calibrators.

In recent years this technique has become more popular with an increasing number of successful applications which approached the thermal noise error with existing instruments, and new implementations are being developed to adapt its scientific application to particular domains. For example inverse MultiView, for the cases when the targets are strong masers and the frequency is 6.7GHz (Hyland et al. 2022, 2023). Additionally it is a very active field of research in the era of next generation interferometers and is a main driver for key multi-pixel capabilities that enable simultaneous observations of the target and multiple calibrators (Rioja & Dodson 2020).

Conventional Multiview (cMV) introduced in Rioja et al. (2017) is optimized for precise astrometric studies in observations where the atmospheric spatial structure changes are dominant, e.g. low frequencies (<5 GHz), low elevations and/or the longest baselines, among others. The scheduling constraints for precise sampling of the dominant spatial structure results in a high density of calibration scans within the coherence time, i.e. it imposes a high calibration overhead leading to low fractional on-target time, in general. At mid-frequencies ($\sim 5-8$ GHz), where the atmospheric temporal structure is the dominant systematic error, such a sequence can be surplus to requirements; In these cases alternative schedules with greater on-target observing time could be more effective and have the potential for improved results. The limit of applicability of this method is when the coherence time is shorter than the duration of the calibrator scans sequence i.e. high frequencies (>8 GHz), Finally, the successful analysis using multiple calibrators requires phase connections between the calibrator scans used to define each plane. A-priori errors can lead to incorrect phase connection, or “phase ambiguity” problems (i.e. wrapping past $\pm 2\pi$), due to the large residual delays, as discussed in Reid (2022, Sect. 3-4).

In this paper, we propose a new approach, serial MultiView (sMV), to expand the benefits of multiple calibrators introduced in Rioja et al. (2017) to the higher frequency (≥ 5 GHz) including weak sources domain, additionally with a user-friendly tool that makes the analysis robust and accessible to a general VLBI user. The

method of sMV is introduced in Sect. 2. In Sect. 3, we compare the results of PR, cMV, and sMV with the same observation data. In sect. 4, we discuss the key advantages and observation scheduling of sMV. Finally, we summarize and look into further application and development in Sect. 5.

2. METHOD

The general idea of sMV is a variant of PR with extra spatial-structure phase correction. For PR, the phase difference between the target and the only phase calibrator is considered small. So, the phases estimated through fringe fitting with the calibrator are directly applied to the target. This works fine if the angular separation between the target and the calibrator is small; however, it is not always possible to find a calibrator close enough to the target. In the case of a large angular separation, if the residual spatial structure is not corrected, image quality may degrade and there may be systematic errors in position measurement.

Within an area of approximately a few degrees, the residual spatial structure can be approximated with linear gradients, i.e., a phase plane in a 3-dimensional Cartesian space with RA, DEC, and phase as axes. For sMV, this plane is estimated through sampling of relative phase differences of several nearby calibrators. The procedure is quite straightforward in the case without phase ambiguity, so we will first introduce the framework in this case, and then discuss how to deal with the tricky ambiguity problem.

2.1. Case without phase ambiguity

There are some basic requirements for data to be processed using sMV: more than one phase calibrator near the target source; fast switching between all sources or observing simultaneously; at least one (primary) calibrator being strong and compact enough for fringe fitting and having a precise a priori position. For the calibration of data meeting the above requirements, sMV is a step inserted into the standard astrometric VLBI data calibration flow. So, the calibration steps in the standard flow should be done before the application of sMV, including amplitude, EOP, ionosphere, and other calibrations.

After the preparations are completed, the sMV procedure begins. The phase plane is in a 3-dimensional space: RA, DEC, and phase as X , Y , and Z axes respectively. The primary calibrator is fixed at the original point $(0, 0, 0)$, and the phase plane keeps passing through it. Then, fringe fit with the primary calibrator and apply to all other (secondary) calibrators because the phase of the primary calibrator is taken as the

zero reference. On this basis, fringe fitting is done for each secondary calibrator to obtain residual phases of them. In this subsection, it is assumed that the residual phases never exceed $\pm\pi$ for simplification. The time series for secondary calibrators can then be expressed as $\{(x, y, \phi, t)_i, i = 1 \dots s\}$, where (x, y) is the relative position, ϕ and t denote residual phase and time respectively, while s is the total scan number of secondary calibrators.

Next, an iteration is performed along the time series. The initial normal vector of the phase plane is set to be $(0, 0, 1)$. The phase plane is rotated once at each iteration to pass through the new point $(x, y, \phi)_i$. Based on the current phase plane, only a small rotation angle is needed under the assumption of a steady and slow-changing spatial structure on a time scale of minutes. To minimize the rotation angle, the Euler-Rodrigues formula (Euler 1776; Rodrigues 1840) is used for the rotation. Fig. 1 is a schematic of the rotation. $\vec{n} \times \text{OA}$ gives the rotation axis \vec{k} , while the rotation angle θ is the angle between OA and the phase plane. During the iteration, the phase plane will quickly converge to the vicinity of the “true” phase plane.

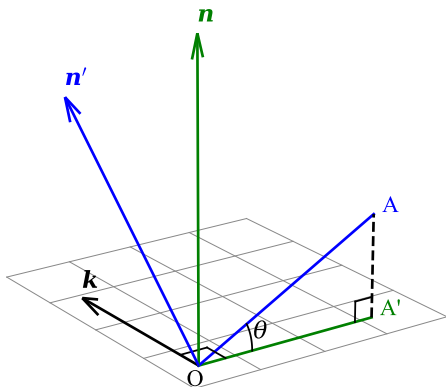


Figure 1. Schematic of phase plane rotation. O is the original point $(0, 0, 0)$ of the 3-dimensional space, and the gridlines denote the phase plane. \vec{n} is the normal vector of the phase plane to be rotated. A is the point that the phase plane is going to pass through. A' is the projection of A on the phase plane. \vec{k} is the rotation axis, θ is the rotation angle, and \vec{n}' is the normal vector after rotation.

At the completion of the iteration, we get a phase plane normal vector time series, which is an approximation of the time-varying spatial-structure residual delay. The next step of sMV is the same as that of cMV: Applying spatial interpolation to obtain the phase correction for the target. All the sMV steps above should be done

for every reference-antenna baseline. Finally, apply the corrected phases to the target, and then imaging and astrometric fitting can be conducted.

2.2. Dealing with phase ambiguity

Phase ambiguity is a common issue in practice and can introduce large biases, so it is essential to detect and correct it during the sMV iteration. Here we give a robust recursive automatic phase ambiguity detection algorithm with the advantage of being resistant to misjudgments caused by outliers. First, we assume no residual phase changes over $\pm 2\pi$ between scans. At each iteration introduced in Sect. 2.1, three directions of phase wrap are “tried”: $+2\pi$, ± 0 , or -2π . Recursively, for each direction, three further directions can be derived. Thus, for a depth of n , the entire set of explored paths forms a ternary tree with 3^n leaf nodes. Note that the time complexity of the recursion is $O(3^n)$, so the depth should not be large and it is better to prune some branches of the ternary tree according to certain thresholds. A flowchart of the recursive procedure is given in Fig. 2, and a schematic of the ternary tree is shown in Fig. 3.

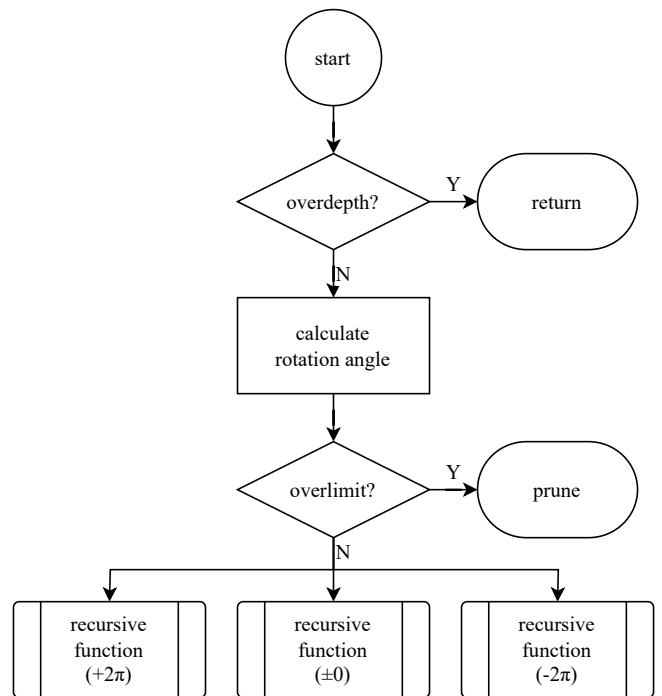


Figure 2. Flowchart of the recursive function.

The direction in the first level of recursion corresponding to the “best” leaf node is chosen as the phase ambiguity solution for each iteration. But how to judge which leaf node is the “Best”? Usually, the phase plane maintains a roughly stable rotational trend over a time

Table 1. Brief information of the example observation

Source Name	RA (h:m:s)	DEC (d:m:s)	σ (mas)	S_{unres} (mJy Beam ⁻¹)	Distance (deg)
J0517+0648*	05:17:51.3442	+06:48:03.210	0.24	0.467 (S)	2.5
J0519+0848	05:19:10.8111	+08:48:56.734	0.21	0.253 (S)	0.93
J0521+1227	05:21:59.7709	+12:27:05.551	0.61	-	3.49
J0532+0732	05:32:38.9985	+07:32:43.345	0.22	0.222 (C)	2.8
V1859 Ori	05:22:54.7927	+08:58:04.679	0.01	-	-

NOTE— Information of the calibrators is collected from Astrogateo (<http://astrogeo.org>, J2000), while that of the target is collected from *Gaia* DR3 (Gaia Collaboration et al. 2023, J2016). Column σ denotes position uncertainty. Column S_{unres} gives the flux density from unresolved components (band in brackets). The calibrator with “*” is used as the primary calibrator for MV and calibrator for PR.

original (sec)	J0532+0732 20	J0521+1227 20	V1859 ORI 50	J0519+0848 20	J0517+0648 30	J0532+0732 20	J0521+1227 20	V1859 ORI 50	J0519+0848 20	J0517+0648 30	J0532+0732 20	J0521+1227 20	V1859 ORI 50	J0519+0848 20	J0517+0648 30
flagged (sec)		J0521+1227 20	V1859 ORI 50		J0517+0648 30	J0532+0732 20		V1859 ORI 50		J0517+0648 30			V1859 ORI 50	J0519+0848 20	J0517+0648 30

Figure 4. Original observing sequence and the flagged sequence. Gray cells are flagged to simulate a 1/3 sampling rate of secondary calibrators. Time length in seconds of each scan is shown in each cell.

segment of original sequence is kept at the beginning to help the iteration converge quickly. In the case of north-south baseline (BR-PT), both antennas had high elevation angles during the whole session, so the residual phase is small, changes slowly and steadily, and there is no phase ambiguity. The estimated phase corrections for target of two sequences are almost the same. While in the case of east-west baseline (HN-PT), one antenna (HN) was affected by low elevation angles. The residual phase changes faster and ambiguity occurs, and the estimated phase correction of flagged sequence slightly loses some of the high-frequency jitters in the time series. This is a foreseeable result, since the sampling rate of secondary calibrators is only 1/3 of the original sequence. But the loss is small (\sim several degrees) and does not have a large impact on interferometric imaging.

The images given by three calibration techniques (PR, cMV, and sMV with original/flagged sequence) are shown in Fig. 6. In the PR image, many artifacts indicate that the phase is not calibrated well, reducing the imaging quality; while in MultiView images, these artifacts are mitigated, and the improvement in the reconstruction of point-like source significantly contributes to the fitting of the astrometric center. This is more pronounced in the east-west direction, as phase ambiguity on east-west baselines is well corrected. The difference between the original and flagged sequence is hard to tell with the naked eye, proving the feasibility of lowering secondary calibrator sampling rate.

The astrometric results of different calibration techniques are listed in Table 2. MultiView results are close to each other in flux density and SNR, and are much better than those of PR. This is as expected, but it’s worth noting that the cMV results are achieved after careful manual ambiguity correction, while sMV can do it semi-automatically. Let’s then compare these results with theoretical thermal limit. The theoretical RMS σ_{thermal} is 42 $\mu\text{Jy}/\text{beam}$ with the eight antennas involved and an on-target time of ~ 36 minutes, calculated using the European VLBI Network (EVN) Observation Planner². Compared to PR being four times the theoretical value, the MultiView values are quite close to the thermal limit.

With the improved SNR, the position formal uncertainties of cMV and sMV are reduced. Notably, there is an inconsistency in the positions measured by the three calibration techniques. This could be due to two factors: reference point differences and residual phase errors. Reference points of the calibration techniques are different because they make use of the a priori positions of calibrators in different ways, while in terms of residual phase errors, consider a case of single baseline: assume wavelength $\lambda = 6$ cm, baseline length $B = 4000$ km, then $\lambda/B \approx 3$ mas, thus a phase difference of 120° results in

² <https://planobs.jive.eu>

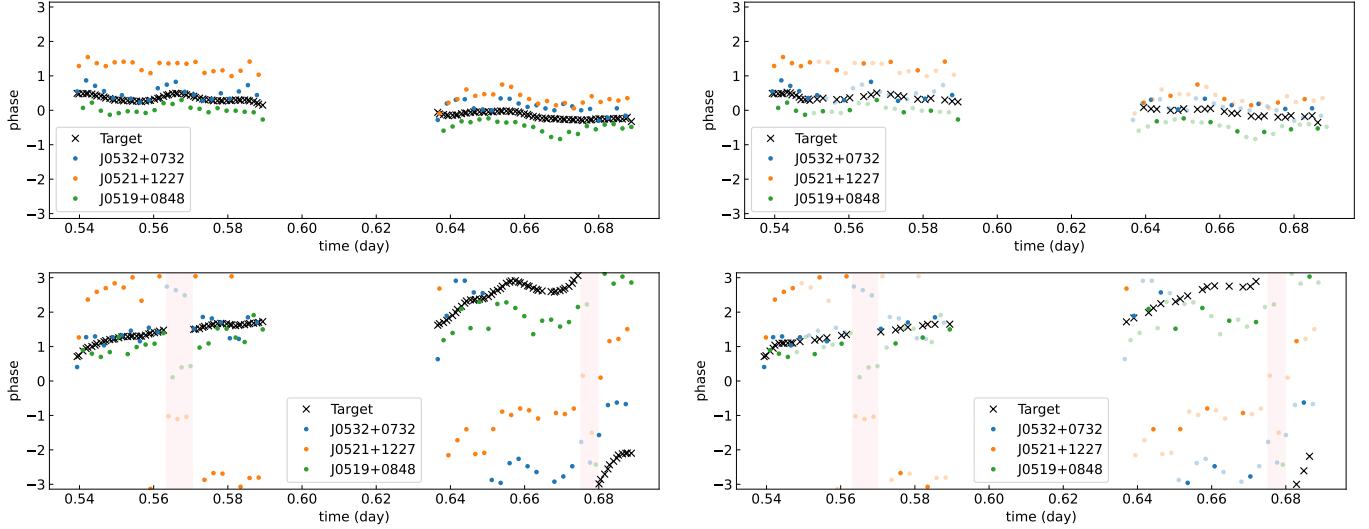


Figure 5. Residual phases in radian of secondary calibrators and estimated phase corrections for target (V1859 Ori). Left panels: original sequences; right panels: flagged sequences. Upper panels: baseline BR-PT; lower panels: baseline HN-PT. Semitransparent calibrator scans are flagged and not used in sMV. Target scans within time ranges with pink background are not used in imaging.

Table 2. Astrometric results of different calibration techniques of V1859 Ori in BZ087B1

Tech.	S_{peak} (mJy Beam $^{-1}$)	SNR	RMS (μ Jy/beam)	RA (h:m:s)	DEC (d:m:s)	$\Delta\alpha^*$ (μ as)	$\Delta\delta$ (μ as)	σ_{RA} (μ as)	σ_{DEC} (μ as)	$\Delta\alpha^*_{\text{Gaia}}$ (μ as)	$\Delta\delta_{\text{Gaia}}$ (μ as)
PR	3.81 ± 0.15	25.62	165	05:22:54.7950173	+08:58:04.479906	896	633	51.7	76.5	1098.1	417.9
cMV	4.68 ± 0.06	81.90	59	05:22:54.7949956	+08:58:04.479763	575	490	13.6	25.1	776.6	274.9
sMV	4.68 ± 0.05	85.54	56	05:22:54.7949568	+08:58:04.479273	-	-	13.0	24.1	201.7	-215.1
sMV*	4.61 ± 0.06	77.01	61	05:22:54.7949585	+08:58:04.479242	25	-31	14.5	26.7	226.9	-246.1

NOTE— S_{peak} denotes peak flux density. $\Delta\alpha^*$ and $\Delta\delta$ are position differences relative to sMV (original sequence) results, and α^* denotes $\alpha \cos \delta$. σ_{RA} and σ_{DEC} are formal uncertainties given by AIPS task JMFIT. columns $\Delta\alpha^*_{\text{Gaia}}$ and $\Delta\delta_{\text{Gaia}}$ give the angular separation between the measured position and *Gaia* position propagated to VLBI epoch.

sMV denotes sMV with flagged sequence.

a position shift of about 1 mas. Therefore, to achieve an accuracy of 0.1 mas level, the residual spatial-structure phase error needs to be corrected to a level below 10° .

It is not easy to tell reference point differences and residual phase errors apart with a single epoch. But they behave different between epochs: reference point differences should keep constant while residual phase errors may change randomly. So we use another epoch (VLBA obs. ID: BZ087B2) close in time to BZ087B1 as a comparison, which was scheduled the same as B1 and was observed on September 11, 2021, and the data reduction procedure is kept the same between epochs. The images of V1859 Ori in BZ087B2 are shown in Fig. 7, and the astrometric results are shown in Table 3. The position offset between PR and sMV changes by > 0.5 mas from

B1 to B2, indicating large random residual phase errors; While the offset between cMV and sMV only changes by $9 \mu\text{as}$ in RA direction and $25 \mu\text{as}$ in DEC direction, within $1\text{-}\sigma$ range. This consistency suggests very little residual random errors of both approaches and the offset is mainly caused by reference point differences.

We also compared the positions with *Gaia* DR3 (Gaia Collaboration et al. 2023). The *Gaia* position needs to be propagated to VLBI epoch with proper motion and parallax. During the propagation, *Gaia* parallax zero-point correction recipe provided by Lindegren et al. (2021) is used, with coefficients given by Ding et al. (2024). Since there is a systematic rotation between the

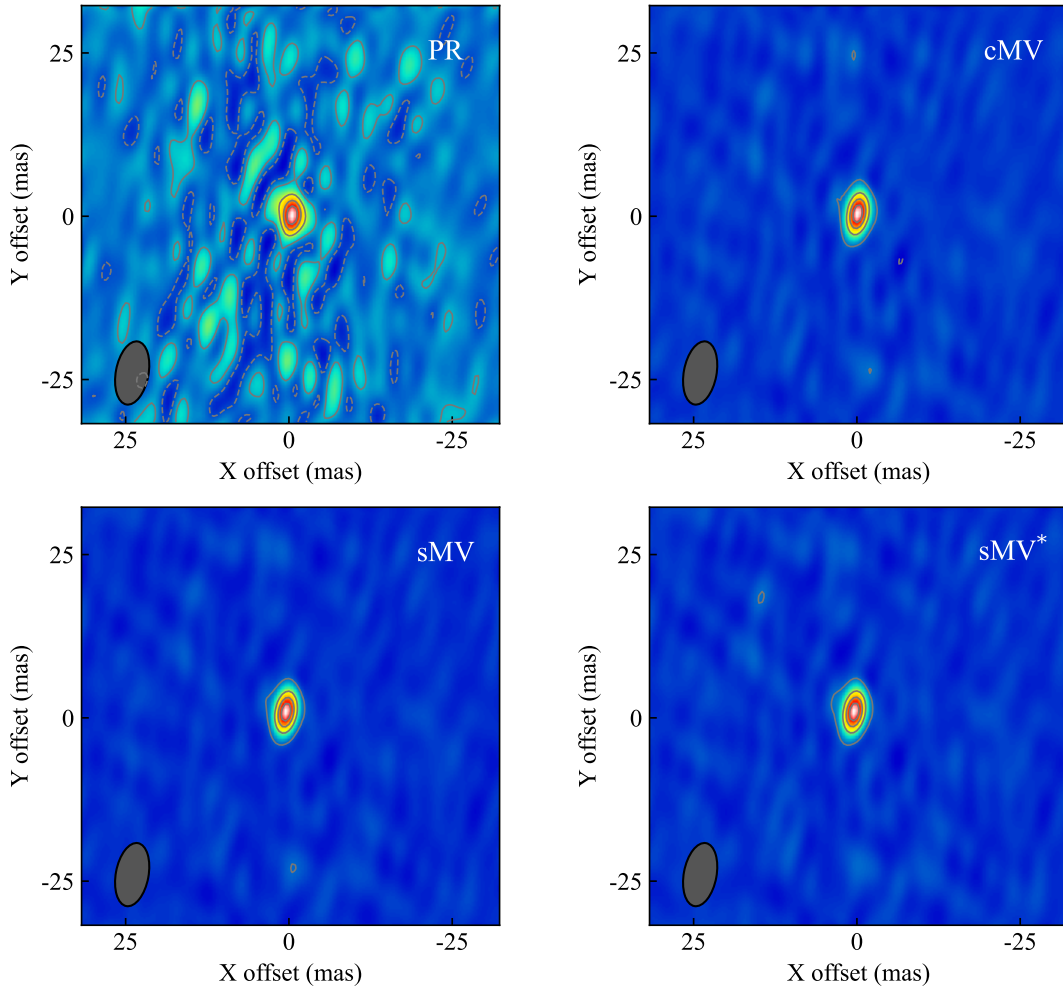


Figure 6. Images of V1859 Ori in BZ087B1 calibrated with different techniques. sMV* denotes sMV with flagged sequence. Image size is 128×128 with a cellsize of 0.5 mas. Contour levels are $[-0.05, 0.05, 0.3, 0.55, 0.8] \times$ peak flux density, in which the -0.05 level is shown in dashed line. The restored beam is shown at the bottom-left corner of each panel.

bright (G band magnitude $G \lesssim 13$) *Gaia* Celestial Reference Frame (*Gaia*-CRF) with respect to the quasars (Lindgren et al. 2018; Brandt 2018), rotation parameters (Zhang et al. 2024) between *Gaia*-CRF3 (*Gaia* Collaboration et al. 2022) and the International Celestial Reference Frame 3 (ICRF3, Charlot et al. (2020)) are also applied. The results are listed in Table 2 and Table 3 and show that the offsets between MultiView positions and propagated *Gaia* position are smaller and more consistent than that of PR, which indicates that there is a better agreement between MultiView VLBI astrometry and *Gaia*. However, since the peak flux centers in radio and optical bands of the star may not be close enough, this is not a definitive conclusion.

The differences between the original and flagged sequences are very small: measured flux densities and SNR of the two sequences are almost the same, and the position difference is also small, in both B1 and B2. It is quite satisfying to achieve comparable results with

only $\sim 1/3$ of sampling rate of secondary calibrators. This proves the potential of sMV in shortening observing cycle and improving on-target time proportion. As a rough estimate, with the time of flagged scans added to on-target time ($1.8\times$), the SNR would go up to ~ 103 for B1 and ~ 58 for B2.

4. DISCUSSION

4.1. Advantages of sMV

Although in principle, in most cases cMV and sMV should provide similar calibration quality for the same data, there are several key advantages of sMV in comparison with the conventional approach, from scheduling to calibration:

ON-TARGET TIME

The application of cMV significantly reduces the on-target time, because all calibrators and the target must be observed repeatedly as a group (e.g., “C1-C2-T-C3-

Table 3. Astrometric results of V1859 Ori in BZ087B2

Tech.	S_{peak} (mJy Beam ⁻¹)	SNR	RMS (μ Jy/beam)	RA (h:m:s)	DEC (d:m:s)	$\Delta\alpha^*$ (μ as)	$\Delta\delta$ (μ as)	σ_{RA} (μ as)	σ_{DEC} (μ as)	$\Delta\alpha^*_{\text{Gaia}}$ (μ as)	$\Delta\delta_{\text{Gaia}}$ (μ as)
PR	1.26 ± 0.03	38.25	34	05:22:54.7950038	+08:58:04.478867	244	380	21.1	45.4	503.6	270.4
cMV	1.29 ± 0.03	42.53	30	05:22:54.7950267	+08:58:04.479002	584	515	15.1	36.0	842.9	405.4
sMV	1.29 ± 0.03	43.99	30	05:22:54.7949873	+08:58:04.478487	-	-	18.0	39.4	259.1	-109.6
sMV*	1.28 ± 0.03	43.34	30	05:22:54.7949879	+08:58:04.478497	9	10	18.2	40.1	268.0	-99.6

NOTE— All columns are kept the same as Table 2.

C4”, repeated). As discussed in Sect. 3, for observations like BZ087, a sequence “C1-C2-T-C1-T-C3-C1-T-C4” has $1.4\times$ on-target time proportion than the original one if the observing cycle is shortened. If we add time to the target instead of shortening observing cycle, the on-target time proportion will even go up to $1.8\times$ that of the original sequence.

COHERENCE TIME LIMIT

The interferometer coherence time is the key limitation to the application of MultiView at higher frequencies (≥ 8 GHz). In the case of Sect. 3, the total time of a cMV group is 140 seconds, while the time interval between two primary calibrator scans of sMV is 100 seconds if the observing cycle is shortened. This makes it possible to apply MultiView at higher frequencies.

LESS SLEW TIME

A lower secondary calibrator sampling rate also means less slew time. This is important not only for time-saving – for large antennas, frequent slewing is potentially damaging to their rotating mechanism.

FLEXIBILITY

sMV provides flexibility in observing sequence and calibrator number. In principle, any number of calibrators (≥ 2) and targets can be combined in any order to meet different needs. It is also possible to use different subsequences in one session, for example, use a lower secondary calibrator sampling rate at high elevation and a higher one at low elevation to maximize efficiency.

AUTOMATICITY

Since the phase plane of each cMV group is fitted independently, fully automatic and accurate identification of outliers and phase wraps is not easy. The iteration along the time axis enables sMV to identify outliers and phase wraps in terms of the continuity and consistency of the time series. The iteration procedure usually does not need any manual intervention, reducing human workload and the potential errors due to subjective judgment.

4.2. Observation scheduling

An important prerequisite for good sMV phase calibration is a well-scheduled observation. Scheduling for different targets should be carefully designed case by case. Factors such as the observing band, the VLBI network used, the target source, calibrators nearby, etc. all have a great influence on scheduling, but there are still some general laws.

The first question to answer is how many calibrators are required. If you can find two nearby calibrators approximately in a line with the target, 1-dimensional phase interpolation can be applied; If three calibrators around the target within $\sim 2^\circ$ can be found, 2-dimensional MultiView is a good choice; If the calibrators are far from the target, it is more robust to add another calibrator for distinguishing phase ambiguity.

The next question is about the sequence. A “full” sampling rate of secondary calibrators (e.g., “C1-C2-T-C3-C4-...” as cMV) provides most details of high-frequency jitters in the residual phase time series, but sacrifices much in terms of on-target time. If there is no low-elevation scenario, e.g., the target Declination is proper for the VLBI network, the session is short, or there are no super long baselines, the atmospheric spatial structure may not change fast. In this case, a lower sampling rate can be used. As discussed above, it is also possible to adopt a hybrid sequence: a higher sampling rate at the beginning and end of the session and a lower sampling rate in the middle.

The above discussion is for traditional VLBI facilities with a single-beam antenna at each site. With advanced or next-generation facilities, there are more scheduling possibilities. For example, for dual-beam systems, duty can be divided between beams. It is theoretically possible to track the target with one beam, and switch between calibrators with another beam. It is even possible to track all sources simultaneously with multi-beam systems, which avoids interpolation in the time domain.

For co-located antennas, i.e., “cluster-cluster” mode (Rioja et al. 1997), the case is similar to multi-beam

systems but offers more flexibilities: sub-array configuration at each site, cooperation between large-but-slow and small-but-fast antennas, and so on. This provides the opportunity to exploit the astrometric performance potential of the VLBI facilities and broaden the applicable frequency range.

5. SUMMARY AND FUTURE OUTLOOK

In this paper, we present a new approach of MultiView, serial MultiView, targeted at overcoming several shortcomings of conventional MultiView approach and provide a user-friendly tool for it. This new approach yields improvements in on-target time proportion and observing cycle length, and provides highly automated phase ambiguity correction.

Comparison through calibrating the same data with PR, cMV, and sMV proves that sMV can achieve significantly improved image quality and astrometric parameters than that of PR, and handles ambiguity problem more automated than cMV. By comparing the results of two epochs, we find that the difference between sMV and cMV mainly comes from the different reference points, while the phase calibration they provide agree very well with each other.

A test for a lower secondary calibrator sampling rate yield a good result, proving that sMV has great potential to shorten observing cycle and increase on-target time proportion without reducing calibration quality significantly. We are going to try different observing sequences, e.g., “C1-T-C2-C1-T-C3-C1-T-C4”, through test observations in the near future. We also plan to test sMV at a higher frequency, e.g., X or Ku band. If the test observations are successful, sMV will be proven to have a potential for a wider application than cMV.

We welcome all VLBI observers to try sMV. The tool we provide makes it very simple to insert sMV into your data reduction flow, and it can significantly improve your imaging quality and astrometry results. It is also valuable for astrophysical research: artifacts in images

decrease with well-calibrated phases. We particularly look forward to a wide application of sMV with next-generation facilities, e.g., the Square Kilometre Array (SKA, Dewdney et al. (2009)) and the next-generation Very Large Array (ngVLA, Carilli et al. (2015)).

1 This work is supported by the National Natural Sci-
2 ence Foundation of China (NSFC) under grant Ns.
3 U2031212, the National Key R&D Program of China
4 (No. 2024YFA1611500), and the Strategic Priority Re-
5 search Program of the Chinese Academy of Sciences,
6 Grant No. XDA0350205.

7 The Python code of sMV procedure can be found
8 at <https://github.com/FrdCHK/serial-MultiView>. We
9 also provide a pipeline for calibration and imaging which
10 can be found through the same URL.

11 VLBA data used in this paper can be downloaded
12 from <https://data.nrao.edu>. This work has made
13 use of data from the European Space Agency (ESA)
14 mission *Gaia* (<https://www.cosmos.esa.int/gaia>), pro-
15 cessed by the *Gaia* Data Processing and Analysis
16 Consortium (DPAC, [https://www.cosmos.esa.int/web/
17 gaia/dpac/consortium](https://www.cosmos.esa.int/web/gaia/dpac/consortium)). Funding for the DPAC has
18 been provided by national institutions, in particu-
19 lar the institutions participating in the *Gaia* Multi-
20 lateral Agreement. The Python package for *Gaia*
21 DR3 parallax zero-point correction developed by P.
22 Ramos can be found at [https://gitlab.com/icc-ub/
23 public/gaiadr3_zeropoint](https://gitlab.com/icc-ub/public/gaiadr3_zeropoint), and the coefficients used in
24 this paper can be found at [https://github.com/yedings/
25 Parallax-bias-correction-in-the-Galactic-plane](https://github.com/yedings/Parallax-bias-correction-in-the-Galactic-plane).

Facilities: VLBA, *Gaia*

Software: Numpy (Harris et al. 2020), Pandas (The pandas development Team 2024), Scipy (Virtanen et al. 2020), Matplotlib (Hunter 2007), Astropy (Astropy Collaboration et al. 2013, 2018, 2022), AIPS (Greisen 2003), ParselTongue (Kettenis et al. 2006).

APPENDIX

A. BZ087B2 IMAGES

The images of V1859 Ori is shown in Fig. 7.

REFERENCES

Astropy Collaboration, Robitaille, T. P., Tollerud, E. J.,
et al. 2013, A&A, 558, A33,
doi: [10.1051/0004-6361/201322068](https://doi.org/10.1051/0004-6361/201322068)

Astropy Collaboration, Price-Whelan, A. M., Sipőcz, B. M.,
et al. 2018, AJ, 156, 123, doi: [10.3847/1538-3881/aabc4f](https://doi.org/10.3847/1538-3881/aabc4f)

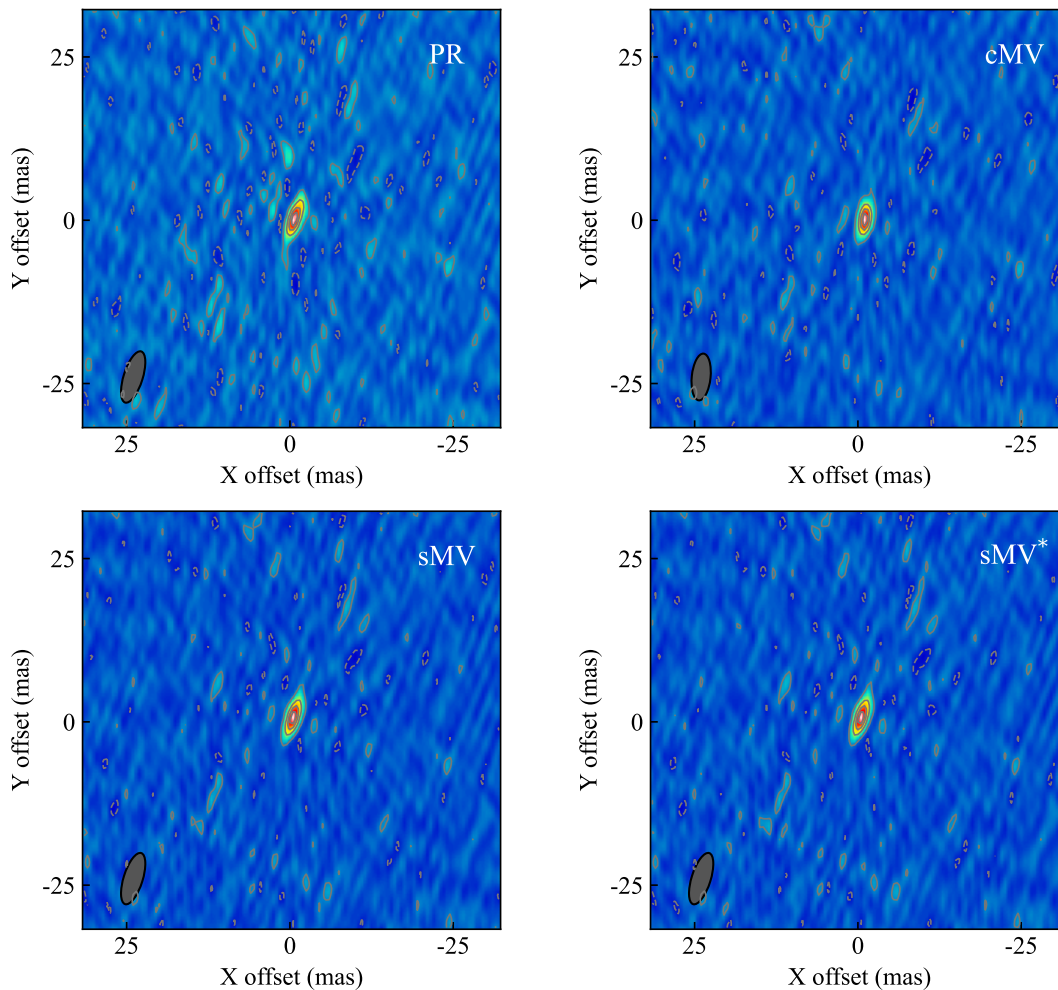


Figure 7. Images of V1859 Ori in BZ087B2 calibrated with different techniques. All elements are kept the same as Fig. 6.

Astropy Collaboration, Price-Whelan, A. M., Lim, P. L., et al. 2022, *ApJ*, 935, 167, doi: [10.3847/1538-4357/ac7c74](https://doi.org/10.3847/1538-4357/ac7c74)

Beasley, A. J., & Conway, J. E. 1995, in *Astronomical Society of the Pacific Conference Series*, Vol. 82, *Very Long Baseline Interferometry and the VLBA*, ed. J. A. Zensus, P. J. Diamond, & P. J. Napier, 327

Brandt, T. D. 2018, *ApJS*, 239, 31, doi: [10.3847/1538-4365/aaec06](https://doi.org/10.3847/1538-4365/aaec06)

Carilli, C. L., McKinnon, M., Ott, J., et al. 2015, arXiv e-prints, arXiv:1510.06438, doi: [10.48550/arXiv.1510.06438](https://doi.org/10.48550/arXiv.1510.06438)

Charlot, P., Jacobs, C. S., Gordon, D., et al. 2020, *A&A*, 644, A159, doi: [10.1051/0004-6361/202038368](https://doi.org/10.1051/0004-6361/202038368)

Dewdney, P. E., Hall, P. J., Schilizzi, R. T., & Lazio, T. J. L. W. 2009, *IEEE Proceedings*, 97, 1482, doi: [10.1109/JPROC.2009.2021005](https://doi.org/10.1109/JPROC.2009.2021005)

Ding, Y., Liao, S., Wu, Q., Qi, Z., & Tang, Z. 2024, *A&A*, 691, A81, doi: [10.1051/0004-6361/202450967](https://doi.org/10.1051/0004-6361/202450967)

Euler, L. 1776, *Novi commentarii academiae scientiarum Petropolitanae*, 208

Gaia Collaboration, Klioner, S. A., Lindegren, L., et al. 2022, *A&A*, 667, A148, doi: [10.1051/0004-6361/202243483](https://doi.org/10.1051/0004-6361/202243483)

Gaia Collaboration, Vallenari, A., Brown, A. G. A., et al. 2023, *A&A*, 674, A1, doi: [10.1051/0004-6361/202243940](https://doi.org/10.1051/0004-6361/202243940)

Greisen, E. W. 2003, in *Astrophysics and Space Science Library*, Vol. 285, *Information Handling in Astronomy - Historical Vistas*, ed. A. Heck, 109, doi: [10.1007/0-306-48080-8_7](https://doi.org/10.1007/0-306-48080-8_7)

Harris, C. R., Millman, K. J., van der Walt, S. J., et al. 2020, *Nature*, 585, 357, doi: [10.1038/s41586-020-2649-2](https://doi.org/10.1038/s41586-020-2649-2)

Hunter, J. D. 2007, *Computing in Science and Engineering*, 9, 90, doi: [10.1109/MCSE.2007.55](https://doi.org/10.1109/MCSE.2007.55)

Hyland, L. J., Reid, M. J., Ellingsen, S. P., et al. 2022, *ApJ*, 932, 52, doi: [10.3847/1538-4357/ac6d5b](https://doi.org/10.3847/1538-4357/ac6d5b)

Hyland, L. J., Reid, M. J., Orosz, G., et al. 2023, *ApJ*, 953, 21, doi: [10.3847/1538-4357/acdbc5](https://doi.org/10.3847/1538-4357/acdbc5)

- Kettenis, M., van Langevelde, H. J., Reynolds, C., & Cotton, B. 2006, in *Astronomical Society of the Pacific Conference Series*, Vol. 351, *Astronomical Data Analysis Software and Systems XV*, ed. C. Gabriel, C. Arviset, D. Ponz, & S. Enrique, 497
- Lestrade, J. F., Rogers, A. E. E., Whitney, A. R., et al. 1990, *AJ*, 99, 1663, doi: [10.1086/115447](https://doi.org/10.1086/115447)
- Lindgren, L., Hernández, J., Bombrun, A., et al. 2018, *A&A*, 616, A2, doi: [10.1051/0004-6361/201832727](https://doi.org/10.1051/0004-6361/201832727)
- Lindgren, L., Bastian, U., Biermann, M., et al. 2021, *A&A*, 649, A4, doi: [10.1051/0004-6361/202039653](https://doi.org/10.1051/0004-6361/202039653)
- Reid, M. J. 2022, *PASP*, 134, 123001, doi: [10.1088/1538-3873/acabe6](https://doi.org/10.1088/1538-3873/acabe6)
- Rioja, M. J., & Dodson, R. 2020, *A&A Rv*, 28, 6, doi: [10.1007/s00159-020-00126-z](https://doi.org/10.1007/s00159-020-00126-z)
- Rioja, M. J., Dodson, R., Orosz, G., Imai, H., & Frey, S. 2017, *AJ*, 153, 105, doi: [10.3847/1538-3881/153/3/105](https://doi.org/10.3847/1538-3881/153/3/105)
- Rioja, M. J., Stevens, E., Gurvits, L., et al. 1997, *Vistas in Astronomy*, 41, 213, doi: [10.1016/S0083-6656\(97\)00008-1](https://doi.org/10.1016/S0083-6656(97)00008-1)
- Rodrigues, O. 1840, *Journal de Mathématiques Pures et Appliquées*, 1e série, 5, 380.
http://www.numdam.org/item/JMPA_1840_1_5__380_0/
- The pandas development Team. 2024, *pandas-dev/pandas: Pandas, v2.2.3*, Zenodo, doi: [10.5281/zenodo.3509134](https://doi.org/10.5281/zenodo.3509134)
- Virtanen, P., Gommers, R., Oliphant, T. E., et al. 2020, *Nature Methods*, 17, 261, doi: [10.1038/s41592-019-0686-2](https://doi.org/10.1038/s41592-019-0686-2)
- Zhang, J., Zhang, B., Xu, S., et al. 2024, *MNRAS*, 529, 2062, doi: [10.1093/mnras/stae705](https://doi.org/10.1093/mnras/stae705)